Highly Efficient Electrocatalytic Oxygen Evolution Over Atomically Dispersed Synergistic Ni/Co Dual Sites

Zhihao Pei; Xue Feng Lu; Huabin Zhang; Yunxiang Li; Deyan Luan; Xiong Wen (David) Lou

2022

Zhihao Pei, Xue Feng Lu, Huabin Zhang, Yunxiang Li, Deyan Luan & Xiong Wen (David) Lou (2022). Highly Efficient Electrocatalytic Oxygen Evolution Over Atomically Dispersed Synergistic Ni/Co Dual Sites. Angewandte Chemie International Edition, 61(40), e202207537-. https://dx.doi.org/10.1002/anie.202207537

https://doi.org/10.1002/anie.202207537

Highly Efficient Electrocatalytic Oxygen Evolution Over Atomically Dispersed Synergistic Ni/Co Dual Sites

Zhihao Pei,† Xue Feng Lu,† Huabin Zhang, Yunxiang Li, Deyan Luan, and Xiong Wen (David) Lou**

[*] Z. H. Pei, Dr. X. F. Lu, Dr. Y. X. Li, Dr. D. Y. Luan, Prof. X. W. Lou
School of Chemical and Biomedical Engineering, Nanyang Technological University, 62 Nanyang Drive, Singapore, 637459, Singapore
Email: dyluan@ntu.edu.sg (D. Y. Luan) ; davidlou88@gmail.com (X. W. Lou)

Prof. H. B. Zhang

KAUST Catalysis Center (KCC), King Abdullah University of Science and Technology (KAUST), Thuwal 23955-6900, Saudi Arabia

† These authors contribute equally to this work.

Abstract

Single-atom catalysts (SACs) are being pursued as economical electrocatalysts. However, their low active-site loading, poor interactions, and unclear catalytic mechanism call for significant advances. Herein, atomically dispersed Ni/Co dual sites anchored on nitrogen-doped carbon (a-NiCo/NC) hollow prisms are rationally designed and synthesized. Benefiting from the atomically dispersed dual-metal sites and their synergistic interactions, the obtained a-NiCo/NC sample exhibits superior electrocatalytic activity and kinetics towards the oxygen evolution reaction. Moreover, density functional theory calculations indicate that the strong synergistic interactions from heteronuclear paired Ni/Co dual sites lead to the optimization of the electronic structure and the reduced reaction energy barrier. This work provides a promising strategy for the synthesis of high-efficiency atomically dispersed dual-site SACs in the field of electrochemical energy storage and conversion.

Keywords: Single-atom catalysts, Dual-metal sites, Synergistic interactions; Hollow prisms, Oxygen evolution reaction.

The severe global energy crisis and continuous environmental degradation make it urgent to develop highly efficient, environmental-friendly, and sustainable energy conversion and storage technologies.[1] As a vital reaction and usually a limiting step in many oxygen-involved electrochemical devices, including water splitting, rechargeable metal-air batteries, and reversible fuel cells, the oxygen evolution reaction (OER) has received widespread attention.[2,3] At present, Ru/Ir-based catalysts are still considered to be the benchmark OER electrocatalysts, but the high cost, low crustal reserve, and relatively poor stability prevent their large-scale application.[4-8] As a result, it is significant to develop low-cost and earth-abundant transition metal-based electrocatalysts as alternatives to noble metals, significantly upgrading the present energy technology landscape.

Although the OER performance of transition metal-based electrocatalysts could be improved by the surface/interface atomic/molecular engineering (e.g., heteroatom-doping, interfacial bonding) and nanostructure engineering,[9-13] they usually suffer from instability and corrosion issues under high potential and harsh OER operating conditions, making it difficult to recognize the active sites. Fortunately, single-atom catalysts (SACs) with uniformly dispersed reactive centers in highly controllable and nearly identical configurations provide us an elegant platform to identify the nature of the reactive centers and understand the catalytic mechanisms at the atomic level.[14-17] As one popular material system in SACs, metal-nitrogen-carbon (M-N-C) materials have made great strides in terms of synthetic methods, structural characterizations, and catalytic applications.[18,19] However, the metal sites in most reported M-N-C materials are homonuclear with relatively low loading, resulting in unsatisfactory catalytic activity.[20,21] On the other hand, the matrixes (including carbon materials and inorganic compounds) supporting these atomic metal sites typically have a low specific

surface area, which is not conducive to the uniform dispersion of metal sites, as well as the charge and mass transfer during the electrocatalytic process.[22] A recent study shows that the introduction of additional metal sites can induce strong synergistic interactions to boost the electrocatalytic performance.[23] However, how to uniformly disperse these metal sites in the matrix at the atomic level and reveal the intrinsic mechanism of the performance improvement through precise structural characterization and theoretical calculation remains a major challenge.

Based on the above analysis and guidance, herein, atomically dispersed Ni/Co dual sites anchored on nitrogen-doped carbon (denoted as a-NiCo/NC) hollow prisms via a multi-step templating approach involving an atom migration-trapping process are rationally designed and synthesized. The elaborately controlled atomization process of NiCo nanoparticles (NPs) within nitrogen-doped carbon (NC) hollow prism ensures atomically uniform dispersion of metal sites. The dual-metal sites with heteronuclear Ni-Co atomic pairs induce strong synergistic interactions to boost the OER activity through manipulating the electronic structure and lowering the reaction energy barrier, as evidenced by density functional theory (DFT) calculations. Thus, the obtained a-NiCo/NC sample delivers superior OER performance with an overpotential of 252 mV at 10 mA cm^{-2}, a small Tafel slope of 49 mV dec^{-1}, and long-term durability over 150 h in alkaline electrolyte, which is much better than that of several control samples including atomically dispersed single-metal-site samples, NiCo NPs encapsulated into NC (NiCo NPs/NC) hollow prisms, and even commercial RuO_2.

The synthetic approach for the a-NiCo/NC is illustrated in **Figure 1**. First, uniform NiCo-based acetate hydroxide precursor (denoted as NiCo-precursor) prisms with an average length of 600 nm (Figures S1 and S2, Supporting Information (SI)) are synthesized according to our previous work

with some modifications.[24] Then a thin polydopamine (PDA) layer is uniformly grown on the surface of prisms through self-polymerization in an alkaline ethanol solution, generating NiCo-precursor/PDA core-shell prisms (Figure S3, SI). The obtained NiCo-precursor/PDA prisms are redispersed in 10 mL of deionized water. After continuous stirring for 2 h at 60 °C, the inner NiCo-precursor cores could be partially etched, generating hollow NiCo-precursor/PDA prisms (Figure S4, SI). These hollow NiCo-precursor/PDA prisms are firstly carbonized at a low temperature, and after removing the excessive metal particles in an acidic solution, the NiCo NPs/NC sample is obtained. These NiCo NPs/NC particles are subsequently evolved into the final a-NiCo/NC hollow prisms through an atom migration-trapping process at a higher temperature (see SI for experimental details). Besides, this synthetic strategy can be applied to synthesize atomically dispersed Ni or Co single sites anchored on NC (denoted as a-Ni/NC and a-Co/NC, respectively) and metal-free NC with a similar structure (Figures S5-S8, SI).

Field-emission scanning electron microscopy (FESEM) images show the well-preserved prism structure of NiCo NPs/NC (**Figure 2**a,b). Transmission electron microscopy (TEM) images and X-ray diffraction (XRD) analysis show that the NiCo NPs are encapsulated into NC hollow prisms (Figure 2c,d; Figures S9 and S10, SI). After the atom migration-trapping process, these NiCo NPs disappear, resulting in formation of a-NiCo/NC hollow prisms (Figure 2e-h), and only the graphitic carbon can be observed in the high-resolution transmission electron microscopy (HRTEM) image (Figure 2i). The disappearance of the XRD diffraction peaks belonging to metals further confirms the successful removal of metal NPs in a-NiCo/NC (Figure S10, SI). Meanwhile, the high-angle annular dark-field scanning transmission electron microscopy (HAADF-STEM) and corresponding elemental

mapping images of a-NiCo/NC reveal that both atomically dispersed Ni and Co elements are uniformly distributed across the entire NC hollow prism (Figure 2j,k). The energy-dispersive X-ray (EDX) line scanning results and the EDX spectrum both verify the existence of the Ni and Co species in a-NiCo/NC (Figures S11 and S12, SI). As shown in Figure 2l, the high density of bright spots in the aberration-corrected HAADF-STEM image confirms the atomically dispersed Ni and Co sites in the a-NiCo/NC catalyst. Interestingly, numerous atomic pairs circled by the orange dash line can be observed, implying the possibly formed Ni/Co dual-metal sites.[25,26] The total metal content in a-NiCo/NC as determined by the inductively coupled plasma optical emission spectrometer (ICP-OES) is found to be 1.60 wt% (0.56 wt% for Ni and 1.04 wt% for Co), which is approximately double of that of a-Ni/NC (0.62 wt%) and a-Co/NC (0.65 wt%) samples (Table S1, SI). The higher metal loading capacity of a-NiCo/NC may be due to the interactions between Ni and Co species to stabilize each other.[25] Besides, the atomization process endows a larger Brunauer-Emmett-Teller (BET) specific surface area of 338.6 m^2 g^{-1} for a-NiCo/NC compared to 155.4 m^2 g^{-1} for NiCo NPs/NC (Figure S13, SI), which may be due to the generation of micro/meso pores during the further carbonization at the higher temperature associated with some partial carbon loss,[27] thus facilitating the exposure of the active sites. Meanwhile, a higher intensity ratio of D and G bands (I_D/I_G) for carbon in a-NiCo/NC implies that high-temperature calcination will produce more defects in the carbon matrix (Figure S14, SI), which has also been proven beneficial for electrocatalysis.[28]

X-ray photoelectron spectroscopy (XPS) and X-ray absorption fine spectroscopy (XAFS) are used to investigate the chemical state and coordination environment. The high-resolution N 1s XPS spectra show the obvious metal-N peak (~399.5 eV) in the three atomically dispersed metal-site

samples compared with the NC sample, which suggests that the metal-N bonds are the main coordination for the metal sites anchored on carbon (Figure S15, SI).[29] A higher ratio of N content in the form of metal-N species in a-NiCo/NC (25.9%) than that of a-Ni/NC (11.8%) and a-Co/NC (12.3%) verifies that a-NiCo/NC has a higher metal content, in line with the ICP-OES results. Moreover, the higher relative N content in the form of metal-N will induce more metal-N interactions, which is critical for the stabilization of single atoms and their catalytic performance.[30] The peak-fitting analysis of Ni 2p and Co 2p spectra (Figure S16, SI) suggests that two chemical states exist in NiCo NPs/NC, corresponding to the spin-orbital characteristics of the metallic state (853.1 eV for Ni $2p_{3/2}$ and 870.5 eV for Ni $2p_{1/2}$; 778.0 eV for Co $2p_{3/2}$ and 792.8 eV for Co $2p_{1/2}$) and oxidation state (855.4 eV for Ni $2p_{3/2}$ and 873.5 eV for Ni $2p_{1/2}$; 781.0 eV for Co $2p_{3/2}$ and 796.8 eV for Co $2p_{1/2}$), accompanied with a pair of broad satellite peaks. In contrast, there is only one chemical state between zero and divalent for Ni 2p and Co 2p in a-Ni/NC and a-Co/NC, respectively, which is in line with the reported valence of SACs.[31,32] A more comprehensive understanding of the metal coordination environment is obtained by X-ray absorption near-edge structure (XANES) and extended X-ray absorption fine structure (EXAFS) measurements. **Figure 3**a,b show the k^2-weighted Fourier transform (FT) EXAFS of a-NiCo/NC and its references at Co and Ni *K*-edges. The dominant metal-N coordination (peak at 1.42 Å for Ni-N bonds, 1.47 Å for Co-N bonds) suggests the existence of atomically dispersed Ni and Co atoms in a-NiCo/NC. And the above coordination demonstrates the existence of metal-N interactions, which can stabilize the single atoms in the system and promote their electrocatalytic activity and stability.[33] Moreover, compared to the Ni-Ni bonds (2.05 Å) in Ni foil and the Co-Co bonds (2.07 Å) in Co foil, the peak at 2.23 Å with an obvious shift can be attributed

to Ni-Co bonds, which confirms the existence of heteronuclear Ni-Co dual-site coordination in a-NiCo/NC.[25,26,34] The Co and Ni *K*-edge XANES spectra of a-NiCo/NC, NiCo NPs/NC, and their reference materials are shown in Figure 3c,d. The absorption threshold (marked in the pink area) of a-NiCo/NC is situated between its corresponding metal foil and metal oxide, identifying the oxidized nature of $Ni^{\delta+}$ ($0<\delta<2$) and $Co^{\gamma+}$ ($0<\gamma<3$). Additionally, the wavelet transform (WT) EXAFS contour plots of Ni *K*-edge and Co *K*-edge for a-NiCo/NC both display a maximum intensity at approximately 4 $Å^{-1}$, matching the coordination of Ni-N and Co-N. Meanwhile, the heteronuclear Ni-Co dual-site coordination in a-NiCo/NC can also be corroborated by a sub-maximal intensity at around 5.2 $Å^{-1}$, which has an evident offset compared with the metal-metal coordination in Ni foil and Co foil (Figure 3e).

Electrochemical OER measurements are carried out in 1.0 M KOH solution to evaluate the electrocatalytic performance of a-NiCo/NC, with NiCo NPs/NC, a-Ni/NC, a-Co/NC, and commercial RuO_2 catalysts as references. Although it has been reported that nitrogen-doped carbon can provide active sites for OER,[35] its contribution to electrocatalytic activity is negligible compared to metal sites, which can be seen from the linear sweep voltammetry (LSV) curve of the NC sample (Figure S17, SI). LSV curves show that the a-NiCo/NC sample exhibits the smallest onset overpotential (η_0) of around 198 mV and constantly highest current density throughout the applied potential range (**Figure 4**a). Impressively, as shown in Figure 4b, the a-NiCo/NC sample requires the smallest overpotentials of 252 and 282 mV to afford the current densities of 10 and 50 mA cm^{-2}, respectively, which are superior to those of a-Ni/NC (333 and 387 mV), a-Co/NC (354 and 415 mV), NiCo NPs/NC (312 and 379 mV), and RuO_2 (358 and 441 mV). The far superior catalytic activity of a-NiCo/NC

compared to that of NiCo NPs/NC verifies the strong interactions between nitrogen and dual-metal sites in a-NiCo/NC, which are beneficial for OER. On the other hand, compared with a-Ni/NC and a-Co/NC, the significantly reduced overpotentials of a-NiCo/NC suggest the synergistic catalytic effect between Ni and Co atoms. To obtain some insights into the OER kinetics, Tafel plots of these catalysts are investigated. As shown in Figure 4c, the a-NiCo/NC sample exhibits the smallest Tafel slope of 49 mV dec^{-1}. The impressive OER activity and kinetics thus render a-NiCo/NC one of the most efficient SACs towards OER in alkaline medium (Table S2, SI).[19,25,26,36-50] To further elucidate the intrinsic mechanism for the enhancement of OER activity, per-site turnover frequency (TOF) is calculated based on the assumption that all metal atoms are active sites. Figure 4d shows the enhanced intrinsic activity in a-NiCo/NC with an average five-fold improvement compared to a-Ni/NC and a-Co/NC at the overpotentials from 250 to 325 mV. In addition, due to the close relationship with the amount of exposed active sites, the electrochemical double-layer capacitance measured by the cyclic voltammetry curves at different scan rates can be obtained to evaluate the electrochemically active surface area (ECSA) of these catalysts (Figures S18 and S19, SI). As shown in Figure 4e, a-NiCo/NC exhibits a large specific capacitance (C_{dl}) value of 3.93 mF cm^{-2}, significantly superior to that of a-Ni/NC (1.73 mF cm^{-2}), a-Co/NC (1.44 mF cm^{-2}), and NiCo NPs/NC (1.69 mF cm^{-2}). Furthermore, the ECSA-normalized LSV curves (Figure S20, SI) show the best intrinsic OER activity for a-NiCo/NC. Besides, the electrochemical impedance spectroscopy (EIS) results indicate that the a-NiCo/NC sample also exhibits the lowest charge transfer resistance among these samples (Figure S21, SI), in good agreement with the smallest Tafel slope. Overall, the significantly improved catalytic activity and kinetic process of a-NiCo/NC fully confirm the synergistic interactions of Ni/Co dual

sites on the promotion of OER activity, which will be further discussed in the following theoretical calculations. Additionally, compared with the NiCo NPs/NC and RuO_2 samples, the a-NiCo/NC electrocatalyst exhibits excellent OER durability with a negligible increase in potential after a long-term OER operation for over 150 h in alkaline solution (Figure 4f). The outstanding durability of a-NiCo/NC compared with NiCo NPs/NC could stem from its unique metal-N interactions which stabilize its metal active sites.[51] The nearly unchanged LSV curve, morphology and structural characteristics of a-NiCo/NC after the OER test also demonstrate its high stability (Figures S22-S26, SI).

To further explore the promotion of synergistic interactions of Ni/Co dual sites on the OER activity, some DFT calculations are performed. According to the XAFS and HAADF-STEM results, a Ni/Co dual-site model ($NiCoN_6$) and two single-metal-site models (Ni-N_4, Co-N_4) are constructed (Figures S27-S29, SI).[26,34,38,52] First, the total density of states (DOS) analysis reveals that the bandgap of a-NiCo/NC is reduced a lot compared to that of a-Ni/NC and a-Co/NC (Figure S30, SI). This suggests the improved electronic conductivity in a-NiCo/NC, which is beneficial for the charge transfer during OER, thus resulting in improved OER kinetics.[53] Meanwhile, the calculated partial density of states (PDOS) shows that both Ni 3d and Co 3d of a-NiCo/NC have the substantial DOS in the sharing range from -4 to 2 eV, suggesting the strong electronic coupling between Ni and Co atoms (**Figure 5**a,b).[54] In addition, compared with the Co d-band center for a-Co/NC and the Ni d-band center for a-Ni/NC, the Co and Ni d-band centers for a-NiCo/NC can be observed with an obvious upshifting to Fermi level after the construction of Ni/Co dual sites. As a result, the electronic structure of Ni and Co atoms for a-NiCo/NC could be effectively regulated with more antibonding

states which would enable the active sites to have a stronger binding ability with reactive intermediates, thus facilitating the OER.[55,56] The free energies of each elementary step are calculated to obtain the rate-determining step (RDS) and evaluate the limiting reaction barrier during the OER process.[57] The calculation results show that the RDS of both a-Ni/NC and a-Co/NC is the formation of *O, while the RDS of a-NiCo/NC changes to the formation of *OOH (Figure 5c). The overall reaction overpotential of a-NiCo/NC (0.34 V) is much smaller than that of a-Ni/NC (0.42 V) and a-Co/NC (0.49 V), suggesting the enhanced OER activity of a-NiCo/NC (Figure 5c). Based on the RDS analysis, the a-NiCo/NC presents the optimum theoretical OER performance, thus its most favorable OER pathways are proposed (Figure 5d). The above theoretical calculation results indicate that the strong synergistic interactions originating from the heteronuclear Ni-Co pairs can lower the reaction energy barrier for the OER by manipulating the electronic structure of the dual-site active centers, leading to the enhanced OER activity in comparison to the single-metal-site counterparts.

In summary, we have designed and synthesized atomically dispersed Ni/Co dual sites anchored on nitrogen-doped carbon (a-NiCo/NC) hollow prisms by an elaborate multi-step templating approach involving the atom migration-trapping process. The electrochemical measurements and theoretical calculations demonstrate that the a-NiCo/NC electrocatalyst exhibits excellent OER kinetics and activity, as well as long-term stability due to the delicately designed atomic dual-metal sites and their strong synergistic interactions. This work provides a promising strategy to significantly improve the electrocatalytic performance of single-atom catalysts by constructing heteronuclear dual-metal sites, thereby facilitating their large-scale applications in practical energy storage and conversion technologies.

Acknowledgements

X.W.L. acknowledges the funding support from the Ministry of Education of Singapore through the Academic Research Fund (AcRF) Tier-2 grant (MOE2019-T2-2-049). The authors thank Dr. Shibo Xi and the X-ray absorption fine structure for catalysis (XAFCA) beamline of the Singapore Synchrotron Light Source (SSLS) for supporting the XAFS measurements.

References

[1] S. C. Peter, *ACS Energy Lett.* **2018**, *3*, 1557.

[2] J. Zhang, G. Chen, K. Müllen, X. Feng, *Adv. Mater.* **2018**, *30*, 1800528.

[3] H. Wang, H.-W. Lee, Y. Deng, Z. Lu, P.-C. Hsu, Y. Liu, D. Lin, Y. Cui, *Nat. Commun.* **2015**, *6*, 7261.

[4] Y. Li, Y. Sun, Y. Qin, W. Zhang, L. Wang, M. Luo, H. Yang, S. Guo, *Adv. Energy Mater.* **2020**, *10*, 1903120.

[5] J. Rong, J. Xu, F. Qiu, Y. Zhu, Y. Fang, J. Xu, T. Zhang, *Adv. Mater. Interfaces* **2019**, *6*, 1900502.

[6] X. Wang, L. Yu, B. Y. Guan, S. Song, X. W. Lou, *Adv. Mater.* **2018**, *30*, 1801211.

[7] Y. Huang, S. L. Zhang, X. F. Lu, Z.-P. Wu, D. Luan, X. W. Lou, *Angew. Chem. Int. Ed.* **2021**, *60*, 11841.

[8] L. Yu, J. F. Yang, B. Y. Guan, Y. Lu, X. W. Lou, *Angew. Chem. Int. Ed.* **2018**, *57*, 172.

[9] Y. P. Zhu, C. Guo, Y. Zheng, S.-Z. Qiao, *Acc. Chem. Res.* **2017**, *50*, 915.

[10] H. Xu, H. Shang, C. Wang, Y. Du, *Coord. Chem. Rev.* **2020**, *418*, 213374.

[11] Z. Li, S. Ji, Y. Liu, X. Cao, S. Tian, Y. Chen, Z. Niu, Y. Li, *Chem. Rev.* **2020**, *120*, 623.

[12] B. Y. Guan, X. Y. Yu, H. B. Wu, X. W. Lou, *Adv. Mater.* **2017**, *29*, 1703614.

[13] X. F. Lu, Y. Fang, D. Luan, X. W. Lou, *Nano Lett.* **2021**, *21*, 1555.

[14] H. Zhang, Y. Liu, T. Chen, J. Zhang, J. Zhang, X. W. Lou, *Adv. Mater.* **2019**, *31*, 1904548.

[15] Q. Wang, X. Huang, Z. L. Zhao, M. Wang, B. Xiang, J. Li, Z. Feng, H. Xu, M. Gu, *J. Am.*

Chem. Soc. **2020**, *142*, 7425.

[16] H. Zhang, X. F. Lu, Z.-P. Wu, X. W. Lou, *ACS Cent. Sci.* **2020**, *6*, 1288.

[17] D. Zhao, Z. Zhuang, X. Cao, C. Zhang, Q. Peng, C. Chen, Y. Li, *Chem. Soc. Rev.* **2020**, *49*, 2215.

[18] C. Xin, W. Shang, J. Hu, C. Zhu, J. Guo, J. Zhang, H. Dong, W. Liu, Y. Shi, *Adv. Funct. Mater.* **2022**, *32*, 2108345.

[19] B. Hu, A. Huang, X. Zhang, Z. Chen, R. Tu, W. Zhu, Z. Zhuang, C. Chen, Q. Peng, Y. Li, *Nano Res.* **2021**, *14*, 3482.

[20] C. Zhu, S. Fu, Q. Shi, D. Du, Y. Lin, *Angew. Chem. Int. Ed.* **2017**, *56*, 13944.

[21] W. Sangkhun, J. Ponchai, C. Phawa, A. Pengsawang, K. Faungnawakij, T. Butburee, *ChemCatChem* **2022**, *14*, e202101266.

[22] W. Zang, Z. Kou, S. J. Pennycook, J. Wang, *Adv. Energy Mater.* **2020**, *10*, 1903181.

[23] W. Zhang, Y. Chao, W. Zhang, J. Zhou, F. Lv, K. Wang, F. Lin, H. Luo, J. Li, M. Tong, *Adv. Mater.* **2021**, *33*, 2102576.

[24] L. Yu, L. Zhang, H. B. Wu, X. W. Lou, *Angew. Chem. Int. Ed.* **2014**, *53*, 3711.

[25] Z. Zeng, L. Y. Gan, H. Bin Yang, X. Su, J. Gao, W. Liu, H. Matsumoto, J. Gong, J. Zhang, W. Cai, Z. Zhang, Y. Yan, B. Liu, P. Chen, *Nat. Commun.* **2021**, *12*, 4088.

[26] X. Han, X. Ling, D. Yu, D. Xie, L. Li, S. Peng, C. Zhong, N. Zhao, Y. Deng, W. Hu, *Adv. Mater.* **2019**, *31*, 1905622.

[27] Y. Sun, P. A. Webley, *Chem. Eng. J.* **2010**, *162*, 883.

[28] W. Wang, L. Shang, G. Chang, C. Yan, R. Shi, Y. Zhao, G. I. N. Waterhouse, D. Yang, T. Zhang, *Adv. Mater.* **2019**, *31*, 1808276.

[29] J. Gao, H. b. Yang, X. Huang, S.-F. Hung, W. Cai, C. Jia, S. Miao, H. M. Chen, X. Yang, Y. Huang, T. Zhang, B. Liu, *Chem* **2020**, *6*, 658.

[30] H.-Y. Zhuo, X. Zhang, J.-X. Liang, Q. Yu, H. Xiao, J. Li, *Chem. Rev.* **2020**, *120*, 12315.

[31] Y. Zhao, Z. Pei, X. F. Lu, D. Luan, X. Wang, X. W. Lou, *Chem Catal.* **2022**, *2*, 1480.

[32] Y. Li, S. L. Zhang, W. Cheng, Y. Chen, D. Luan, S. Gao, X. W. Lou, *Adv. Mater.* **2022**, *34*, 2105204.

[33] J. Zhang, C. Liu, B. Zhang, *Small Methods* **2019**, *3*, 1800481.

[34] J. Wang, W. Liu, G. Luo, Z. Li, C. Zhao, H. Zhang, M. Zhu, Q. Xu, X. Wang, C. Zhao, Y. Qu, Z. Yang, T. Yao, Y. Li, Y. Lin, Y. Wu, Y. Li, *Energy Environ. Sci.* **2018**, *11*, 3375.

[35] Y. Zhao, R. Nakamura, K. Kamiya, S. Nakanishi, K. Hashimoto, *Nat. Commun.* **2013**, *4*, 2390.

[36] Y. Zheng, Y. Jiao, Y. Zhu, Q. Cai, A. Vasileff, L. H. Li, Y. Han, Y. Chen, S.-Z. Qiao, *J. Am. Chem. Soc.* **2017**, *139*, 3336.

[37] D. Liu, S. Ding, C. Wu, W. Gan, C. Wang, D. Cao, Z. u. Rehman, Y. Sang, S. Chen, X. Zheng, Y. Wang, B. Ge, L. Song, *J. Mater. Chem. A* **2018**, *6*, 6840.

[38] D. Yu, Y. Ma, F. Hu, C.-C. Lin, L. Li, H.-Y. Chen, X. Han, S. Peng, *Adv. Energy Mater.* **2021**, *11*, 2101242.

[39] M. Liu, N. Li, S. Cao, X. Wang, X. Lu, L. Kong, Y. Xu, X.-H. Bu, *Adv. Mater.* **2022**, *34*, 2107421.

[40] J. Zhao, R. Qin, R. Liu, *Appl. Catal., B* **2019**, *256*, 117778.

[41] L. Bai, C.-S. Hsu, D. T. L. Alexander, H. M. Chen, X. Hu, *J. Am. Chem. Soc.* **2019**, *141*, 14190.

[42] Y. He, X. Yang, Y. Li, L. Liu, S. Guo, C. Shu, F. Liu, Y. Liu, Q. Tan, G. Wu, *ACS Catal.* **2022**, *12*, 1216.

[43] J. Chen, H. Li, C. Fan, Q. Meng, Y. Tang, X. Qiu, G. Fu, T. Ma, *Adv. Mater.* **2020**, *32*, 2003134.

[44] L. Zhang, Y. Jia, G. Gao, X. Yan, N. Chen, J. Chen, M. T. Soo, B. Wood, D. Yang, A. Du, X. Yao, *Chem* **2018**, *4*, 285.

[45] X. Zhu, D. Zhang, C.-J. Chen, Q. Zhang, R.-S. Liu, Z. Xia, L. Dai, R. Amal, X. Lu, *Nano Energy* **2020**, *71*, 104597.

[46] M. Xiao, J. Zhu, S. Li, G. Li, W. Liu, Y.-P. Deng, Z. Bai, L. Ma, M. Feng, T. Wu, D. Su, J. Lu, A. Yu, Z. Chen, *ACS Catal.* **2021**, *11*, 8837.

[47] Y.-S. Wei, L. Sun, M. Wang, J. Hong, L. Zou, H. Liu, Y. Wang, M. Zhang, Z. Liu, Y. Li, S. Horike, K. Suenaga, Q. Xu, *Angew. Chem. Int. Ed.* **2020**, *59*, 16013.

[48] Z. Li, H. He, H. Cao, S. Sun, W. Diao, D. Gao, P. Lu, S. Zhang, Z. Guo, M. Li, R. Liu, D. Ren, C. Liu, Y. Zhang, Z. Yang, J. Jiang, G. Zhang, *Appl. Catal., B* **2019**, *240*, 112.

[49] X. Zhou, J. Gao, Y. Hu, Z. Jin, K. Hu, K. M. Reddy, Q. Yuan, X. Lin, H.-J. Qiu, *Nano Lett.*

2022, *22*, 3392.

[50] C. Rong, X. Shen, Y. Wang, L. Thomsen, T. Zhao, Y. Li, X. Lu, R. Amal, C. Zhao, *Adv. Mater.* **2022**, *34*, 2110103.

[51] S. Büchele, Z. Chen, S. Mitchell, R. Hauert, F. Krumeich, J. Pérez-Ramírez, *ChemCatChem* **2019**, *11*, 2812.

[52] G. Luo, Y. Jing, Y. Li, *J. Mater. Chem. A* **2020**, *8*, 15809.

[53] J. Liu, G. Ye, B. v. d. Zee, J. Dong, X. Qiu, Y. Liu, G. Portale, R. C. Chiechi, L. J. A. Koster, *Adv. Mater.* **2018**, *30*, 1804290.

[54] W. Cheng, S. Xi, Z.-P. Wu, D. Luan, X. W. Lou, *Sci. Adv.* **2021**, *7*, eabk0919.

[55] H. B. Tao, L. Fang, J. Chen, H. B. Yang, J. Gao, J. Miao, S. Chen, B. Liu, *J. Am. Chem. Soc.* **2016**, *138*, 9978.

[56] X. Du, J. Huang, J. Zhang, Y. Yan, C. Wu, Y. Hu, C. Yan, T. Lei, W. Chen, C. Fan, J. Xiong, *Angew. Chem. Int. Ed.* **2019**, *58*, 4484.

[57] Z.-P. Wu, H. Zhang, S. Zuo, Y. Wang, S. L. Zhang, J. Zhang, S.-Q. Zang, X. W. Lou, *Adv. Mater.* **2021**, *33*, 2103004.

Figures and Captions

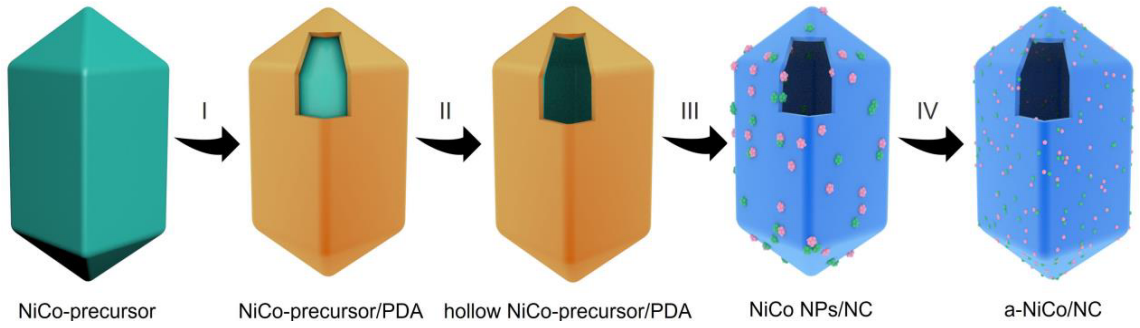

Figure 1. Schematic illustration of the synthesis of a-NiCo/NC. (I) PDA coating on the surface of NiCo-precursor prisms to form NiCo-precursor/PDA core-shell structures. (II) Formation of hollow NiCo-precursor/PDA prisms through the water etching. (III) Formation of NiCo NPs/NC through the annealing treatment in N_2 atmosphere and the acid etching. (IV) Transformation of NiCo NPs/NC by an atom migration-trapping process to form a-NiCo/NC.

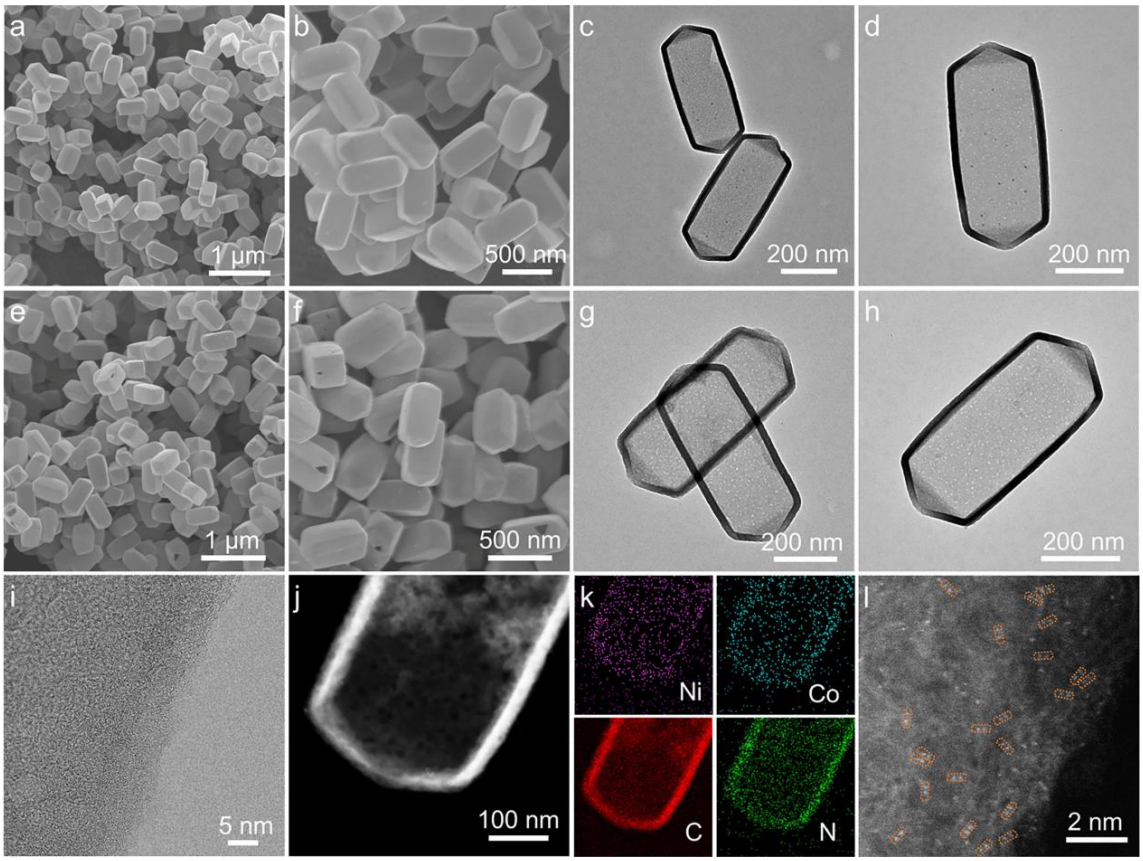

Figure 2. Morphological and structural characterizations. **a,b**) FESEM and **c,d**) TEM images of NiCo NPs/NC. **e,f**) FESEM and **g,h**) TEM images of a-NiCo/NC. **i**) HRTEM image of a-NiCo/NC. **j**) HAADF-STEM and **k**) corresponding elemental mapping images of a-NiCo/NC. **l**) Aberration-corrected HAADF-STEM image of a-NiCo/NC.

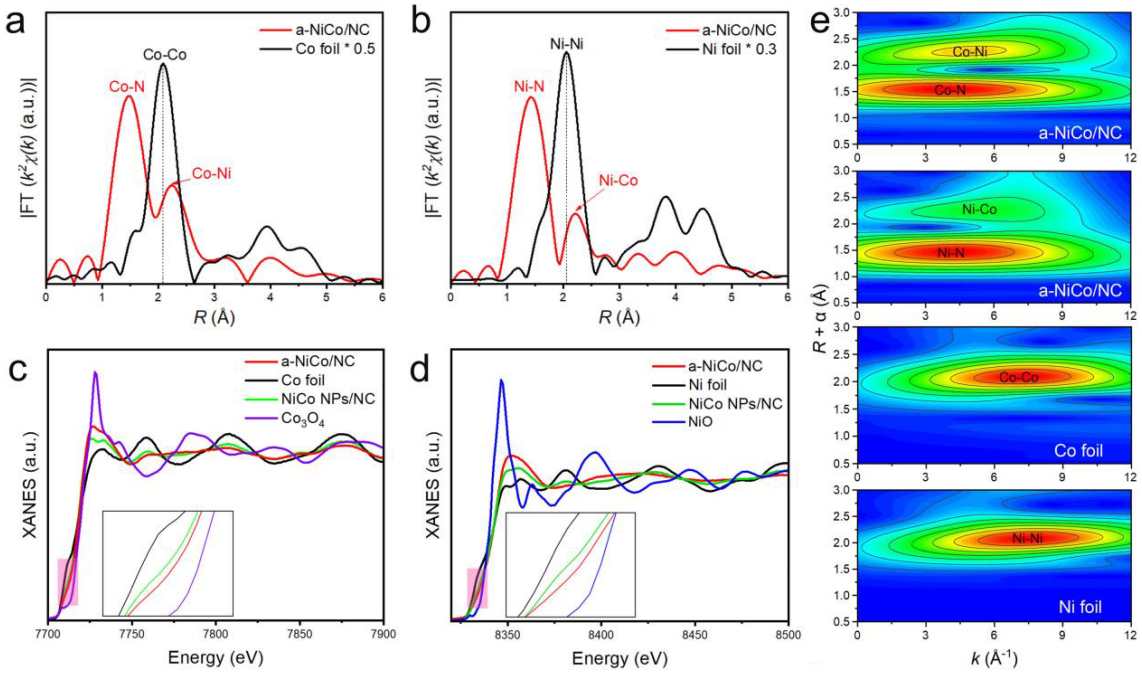

Figure 3. Structural characterization of the catalysts. FT EXAFS spectra of **a**) Co *K*-edge for a-NiCo/NC and Co foil, **b**) Ni *K*-edge for a-NiCo/NC and Ni foil. **c**) Co *K*-edge XANES spectra. **d**) Ni *K*-edge XANES spectra. **e**) WT EXAFS contour plots of Co *K*-edge for a-NiCo/NC, Ni *K*-edge for a-NiCo/NC, Co *K*-edge for Co foil, and Ni *K*-edge for Ni foil.

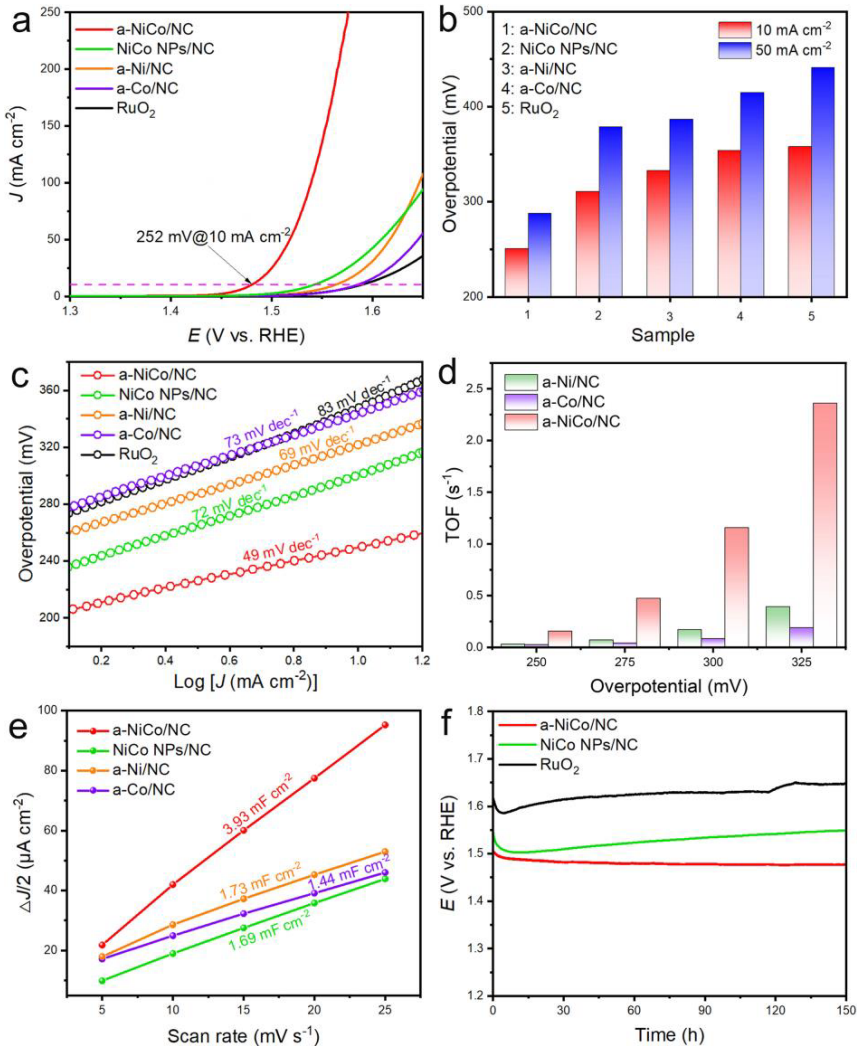

Figure 4. Electrocatalytic OER performance evaluation. **a**) LSV plots, **b**) the corresponding overpotentials at 10 mA cm^{-2} and 50 mA cm^{-2}, **c**) Tafel slopes of a-NiCo/NC, NiCo NPs/NC, a-Ni/NC, a-Co/NC, and RuO_2. **d**) TOF values of a-NiCo/NC, a-Ni/NC, and a-Co/NC. **e**) Capacitive current density ($\triangle J/2$) at 0.94 V vs. RHE against the scan rate for a-NiCo/NC, NiCo NPs/NC, a-Ni/NC, and a-Co/NC. **f**) Potential-time curves at the current density of 10 mA cm^{-2} for a-NiCo/NC, NiCo NPs/NC, and RuO_2.

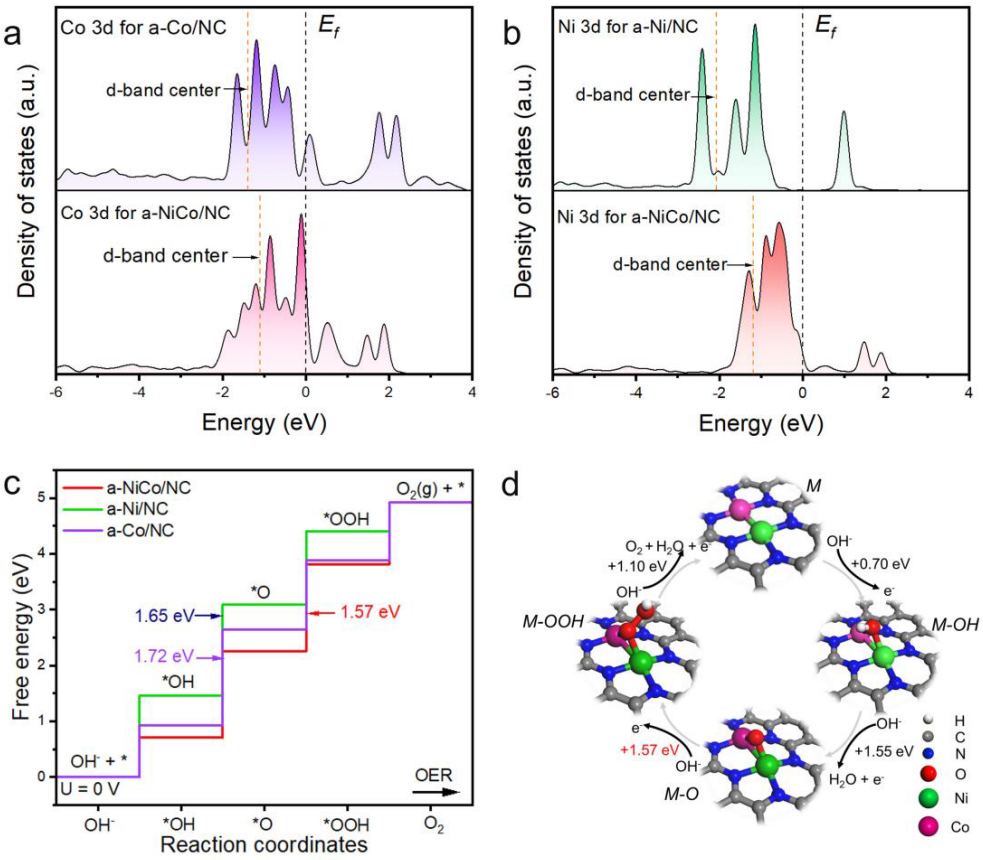

Figure 5. DFT calculation. **a**) Calculated PDOS of Co 3d for a-Co/NC and a-NiCo/NC. **b**) Calculated PDOS of Ni 3d for a-Ni/NC and a-NiCo/NC. **c**) Free energy diagram of OER for a-NiCo/NC, a-Ni/NC, and a-Co/NC. **d**) Schematics of the optimized OER catalytic pathways for a-NiCo/NC.

for Table of Content Entry

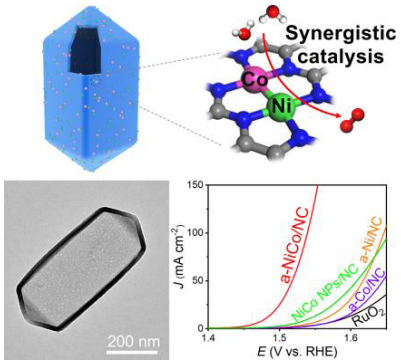

Atomically dispersed Ni/Co dual sites anchored on nitrogen-doped carbon (a-NiCo/NC) hollow prisms are synthesized through a templated assisted atom migration-trapping route. Due to the delicately designed dual-metal sites and their synergistic interactions, the a-NiCo/NC electrocatalyst exhibits significantly improved electrocatalytic oxygen evolution performance compared with atomically dispersed single-metal-site counterparts.